

Optimization of wickless heat pipe heat exchanger using R1234-yf and ethanol as working fluids

Osamah R. Alkhafaj^{1*}, Nabil J. Yasin², Audai H. Al-abbas³

¹ Middle Technical University, Baghdad, Iraq-Technical Instructors Training Institute, Baghdad, Iraq

² Middle Technical University, Baghdad, Iraq -Technical Engineering College Baghdad, Iraq

³ Alfurat Alawsat Technical University, Kufa, Iraq- Technical College Almosaib, Kufa, Iraq

ABSTRACT

This experimental study investigates the use of R1234-yf and ethanol as working fluids in a wickless heat pipe, with air flowing through the heat exchanger ducts. The hot air temperatures were set at 50°C, 55°C and 60°C, while the cold air temperature was fixed at 20°C. Both hot and cold air streams were pumped with Reynolds numbers ranging from 2583 to 20664. The wickless heat pipe was oriented vertically and filled with varying filling ratios of 20%, 40%, 60%, 80% and 100%. The results demonstrate that the wickless heat pipe - heat exchanger achieved the best thermal performance of 0.181 at a filling ratio of 60%, using ethanol as the working fluid and a Reynolds number of 10332. Additionally, a novel approach is proposed to predict the overall thermal performance of the wickless heat pipe - heat exchanger, and the predicted results show good agreement with the experimental findings

Keywords: Thermosiphon, Wickless heat pipe, R1234-yf, Ethanol, Heat exchanger.

OPEN ACCESS


Received: May 12, 2023

Revised: June 16, 2023

Accepted: July 5, 2023

Corresponding Author:

Osamah R. Alkhafaj
osamah.raad@mtu.edu.iq

 **Copyright:** The Author(s). This is an open access article distributed under the terms of the [Creative Commons Attribution License \(CC BY 4.0\)](https://creativecommons.org/licenses/by/4.0/), which permits unrestricted distribution provided the original author and source are cited.

Publisher:

[Chaoyang University of Technology](https://www.chaoyang.edu.cn/)

ISSN: 1727-2394 (Print)

ISSN: 1727-7841 (Online)

1. INTRODUCTION

The wickless heat pipe heat exchanger technology, as investigated by Eidan et al. (2016), offers an active approach to enhance heat dissipation between heat sources and sinks in various applications. In this context, the heat pipe serves as the principal mechanism for transferring heat between the hot and cold fluids within the designated heat exchanger. Consequently, improving the performance of the heat pipe contributes to the overall thermal efficiency of the entire heat exchanger system.

Given the global energy crisis and the detrimental impact of exhaust gases from combustion processes on the environment, the utilization of wickless heat pipes or thermosiphons for cooling electronic components, such as those found in data centers and computers, has become increasingly crucial (Eidan et al., 2016). The enhancement of wickless heat pipe thermal performance plays a pivotal role in meeting these essential requirements and reducing energy consumption associated with cooling processes, as elucidated by Guo and Nutter (2009).

Significant developments in wickless heat pipe technology, particularly in thermosiphons, have aligned with the imperative need for reducing energy dependency in cooling applications. These advancements facilitate the efficient utilization of resources and promote environmentally sustainable cooling practices (Guo and Nutter, 2009).

The thermosiphon or wickless heat pipe typically employs a working fluid for gravity-driven heat transfer from source to sink. This involves pool boiling at the evaporator section, where phase change occurs and vapor bubbles are formed. The movement of these bubbles is influenced by density variations with the surrounding liquid. The vapor

then travels to the adiabatic section, where no heat is added or lost, serving as a transport tunnel between the evaporator and condenser sections. Insulation is crucial in conserving heat energy within the evaporator. The condenser section facilitates condensation and dissipation of heat energy. Gravity aids in the downward flow of the condensed liquid back to the evaporator.

An experimental study by Guo and Nutter (2009) investigated thermosiphons using R-134a and two types of wickless heat pipes, one with a thermal break in the adiabatic section and the other without. The study found that the thermal conductivity of the wall pipe increased the overall heat transfer coefficient of the thermal device. The study also revealed that increasing the applied heat load reduced the effect of axial conduction. The thermosiphon's performance was found to depend directly on the thermophysical properties of the working fluid under fixed operation conditions (Sabharwall and Gunnerson, 2009).

Numerical simulations by Xu et al. (2018) explored the effect of inclination angle on the evaporator's wettability. The results demonstrated that changing the inclination angle from 15° to 90° reduced the thermal resistance of the thermosiphon by 59.9% due to a reduction in bubble accumulation. Additionally, increasing the heat load from 10 to 14 W significantly reduced thermal resistance by 44.1%.

Experimental investigations by Narcy et al. (2018) provided clear visualization of the effect of water boiling in a thermosiphon. The study indicated that the thermosiphon's orientation angle had a minimal impact on its thermal performance. Furthermore, a study on evacuated heat pipes for solar applications found that a filling ratio of 70% resulted in the most active thermal performance (Jafari et al., 2016).

In summary, the thermal performance of wickless heat pipe heat exchangers does not have a definitive governing equation. Thus, efforts are focused on establishing a simple equation or relation that expresses the overall thermal performance using a performance factor, such as the Z-factor. Validation of this achievement requires experimental work encompassing various working fluids and operational conditions.

2. MATERIALS AND METHODS

2.1 Methodology

The present study involves the design, manufacturing, and calibration of a specialized test rig equipped with instruments and devices to measure the thermophysical properties at each state. The findings of this thermal system are discussed herein. Two air ducts have been fabricated in a configuration that allows for a vertically positioned single wickless heat pipe. The lower duct serves to direct hot air towards the evaporator section of the heat pipe, while the upper duct carries cold air to the condenser section. Both ducts are square-shaped with dimensions of 21 × 21 cm to

optimize hydraulic performance (Bhatia, 2001).

The length of the air ducts is 320 cm, and the wickless heat pipe is positioned at an appropriate distance from the entrance to ensure a fully developed flow region for the incoming air (see Fig. 1). It is worth noting that increasing the surface areas of the evaporator and condenser is essential for enhancing heat transfer rates and overall heat exchanger performance. Consequently, fins were incorporated with specific designs and distributions based on previous studies (Kundu and Das, 2009; Yang et al., 2020). The schematic diagram and photographic image of the test rig are illustrated in Figs. 2 and 3 (a), respectively. Additionally, Figs. 3 (b) and (c) depict the photographic image and schematic diagram of the wickless heat pipe, while Fig. 3 (d) shows the positioning of the thermocouples along the heat pipe at various locations. The general design of the used test rig can be achieved in Figs. 2 and 3 below.

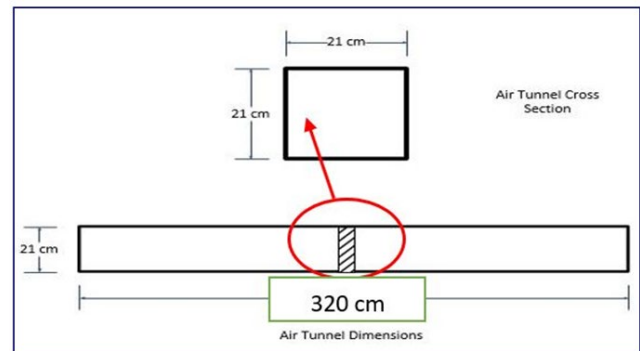


Fig. 1. Schematic diagram of the air duct

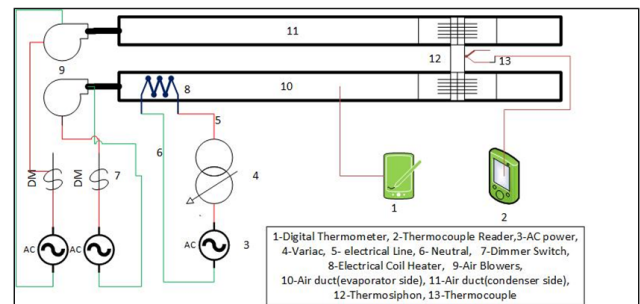


Fig. 2. Schematic diagram of the wickless heat pipe heat exchanger

2.2. Data Reduction

To get more accurate results, the temperature of the evaporator, condenser and adiabatic sections are taken as average values among the readings of thermocouples, as shown in mathematical relations below Ozsoy and Yildirim (2016).

$$T_e = \frac{T_1 + T_2 + T_3 + T_4}{4} \quad (1)$$

$$T_c = \frac{T_7 + T_8 + T_9 + T_{10}}{4} \quad (2)$$

$$T_a = \frac{T_5 + T_6}{2} \quad (3)$$

The consumed heat energy in the evaporator section or the rejected heat one at the condenser section can be conducted depending on Equations 4 and 5, respectively Haider et al. (2002).

$$Q_{eva} = cp_a \dot{m}_a (T_{out,e} - T_{in,e}) \quad (4)$$

$$Q_{con} = cp_a \dot{m}_a (T_{out,c} - T_{in,c}) \quad (5)$$

Regarding that, the present study includes a heat exchanger application, where the heat energy has converted from one fluid to another, so effectiveness is regarded as the performance term. The effectiveness relation is the ratio between actual and maximum heat transfer; therefore, it can be written as shown below Çengel (2009).

$$\varepsilon = \frac{Q_{actual}}{Q_{max}} = \frac{m.C. (T_{h,in} - T_{h,out})}{m.C. (T_{h,in} - T_{c,in})} = \frac{T_{h,in} - T_{h,out}}{T_{h,in} - T_{c,in}} \quad (6)$$

The wickless heat pipe heat exchanger is considered an energy-saving device because it enhances the heat transfer rate by depending on the thermosiphon phenomenon. Then, an energy balance ratio (EBR) is a ratio between the consumed heat energy at the evaporator section to the

rejected heat at the condenser section, as shown in the equation below Haider et al. (2002).

$$EBR = \frac{Q_{eva}}{Q_{con}} \quad (7)$$

The present study aims to fabricate a new relation or equation that assists in predicting the thermal performance of the whole wickless heat pipe heat exchanger by noticing the best operation zone of the referred test rig. Thus, Z-factor is the new fabricated item that includes a dimensionless ratio between the effectiveness and the EBR, as shown in Equation 8. It is essential to discuss the mathematical relation of Z-factor depending on the physics of thermal applications; the highest values of the effects are assumed to be 99.8% or less at the perfect case because there is no ideal heat exchanger. Also, the worst cases of the effectiveness values have not reached the zero because there is not actual operated heat exchanger with zero effectiveness. It is well known that the worst case of heat exchanger may be reached due to low flow rate for the operated fluid and low temperature differences between the hot and cold fluids. But, the heat exchanger body's thermal conductivity still transfers some heat energy from hot to cold regions. This way, the effectiveness doesn't some amounts of heat energy from hot to cold regions, making the effectiveness not reach zero value.

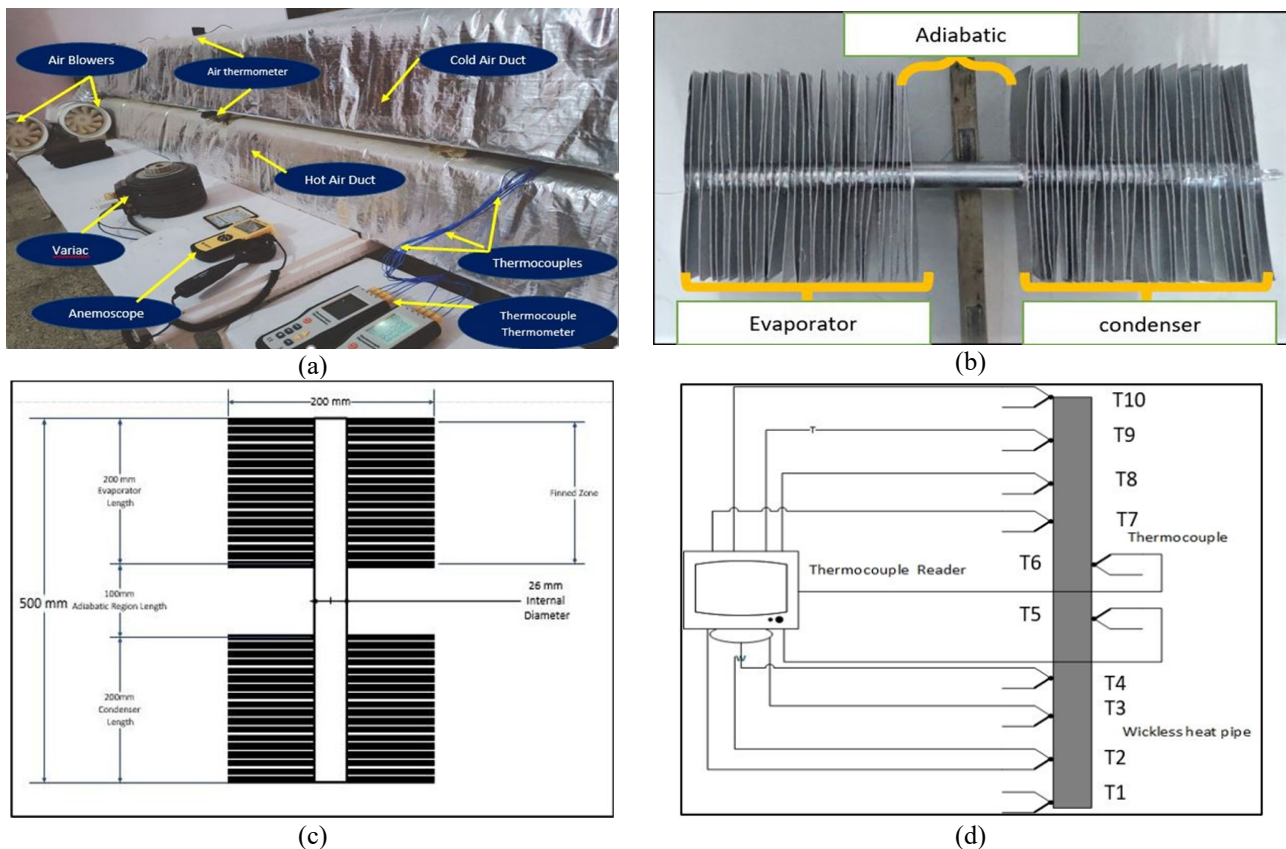


Fig. 3. (a) Test rig with details of the wickless heat pipe; (b) The wickless heat pipe; (c) The wickless heat pipe schematic diagram; (d) Thermocouple distribution on wickless heat pipe length

Moreover, the best value of the EBR can be reached 0.97 or less but doesn't reach the unity because there is no perfect heat transfer without losses. Also, there isn't an actual wickless heat pipe with infinity EBR. Physically, if the heat pipe doesn't work depending on the heat transfer by fluid that is filled with. Then, the thermal conduction of the heat pipe walls tends to transfer some of the heat energy from the evaporator to the condenser. So that, EBR values may reach to the value of 100, 102, 103 or more but not infinity.

According to the previous physics, the new proposed item i.e. Z-factor, can represent the high thermal performance of the wickless heat pipe heat exchanger when there is high effectiveness and lowest EBR as it is shown below:

$$1- \text{For maximum Z-factor} = \frac{\text{effectiveness}}{\text{EBR}} = \frac{99.99}{0.99} = 101 \approx 100$$

$$2- \text{For minimum Z-factor} = \frac{\text{effectiveness}}{\text{EBR}} = \frac{0.001}{1000} = 10^{-6} \approx \text{zero}$$

$$Z\text{-factor} = \frac{\epsilon}{\text{EBP}} \tag{8}$$

The charging of the used wickless heat pipe is governed by the filling ratio that represents the ratio between the charged volume of the used working fluid to the volume of the evaporator section as it is shown in Equation 9.

$$\text{Filling ratio (FR)} = \frac{\text{Vol. of fluid}}{\text{evaporator Vol.}} \tag{9}$$

The variable parameters throughout the present study are listed in Table 1.

Table 1. Variable parameters

No.	Item	Range
1	Inlet hot air temperature (T _{h,in})	50°C, 55°C, 60°C
2	Inlet cold air temperature (T _{c,in})	20°C
3	Reynolds no. (Re. no.)	2583-20664
4	Filling ratios (FR)	20%, 40%, 60%, 80%, 100%
5	Working fluids	Ethanol, R1234-yf

2.3 Uncertainty and Error Analysis

The experimental work includes using measurement devices or instruments to execute the physical performance into logical data that the researchers can understand. Also, the depended instruments during the experimental procedures of the scientific research include some divergence due to continuous utilization, laboratory conditions, etc. Thus, some of the computations are recommended to be done for these instruments in order to check the acceptability of the reading divergence or what are known as error analysis Liu et al. (2019). Kline and McClintock method is considered as one of the well-known methods to satisfy the error analysis requirement (Raad, 2019).

The main measured parameters in the experimental study

are hydraulic diameter, air velocity, atmospheric pressure, air temperature and surface temperature. Therefore, and according to the Kline and McClintock method where measured parameters maximum values and uncertainty of the used instruments should be known as it is shown in the tables below:

Table 2. The uncertainty of the used instrument

Instrument	Uncertainty
Thermocouple thermometer	± 0.1°C
Anemometer	± 0.05 m/s
Power meter	± 0.01 W
Vernier clipper	± 1 mm
Portable barometer	± 1.5 kpa
Bordon gage	± 3.4 kpa
Thermometer	± 0.3°C

Table 3. The values of the measured parameters

Parameter	Value
Duct length	3000 mm
Hydraulic diameter	210 mm
Atmospheric pressure	110 kpa
Maximum applied heat load	2000 W
Ambient temperature	20°C
Maximum surface temperature	50°C
Maximum air velocity	2 m/s

1-uncertainty of the area cross section of the air flow (A = l.w) : l = w = 210 mm.

$$\frac{\partial A}{A} = \sqrt{\left(\frac{\partial l}{l}\right)^2 + \left(\frac{\partial w}{w}\right)^2} = \sqrt{\left(\frac{1}{210}\right)^2 + \left(\frac{1}{210}\right)^2} = 0.0067$$

2-uncertainty of the duct cross section perimeter (P = (l + w) × 2).

$$\frac{\partial P}{P} = \sqrt{\left(\frac{\partial l}{l}\right)^2 + \left(\frac{\partial w}{w}\right)^2} = \sqrt{\left(\frac{1}{210}\right)^2 + \left(\frac{1}{210}\right)^2} = 0.0067$$

3-uncertainty of the hydraulic diameter (Dh = $\frac{4A}{P}$).

$$\frac{\partial Dh}{Dh} = \sqrt{\left(\frac{\partial A}{A}\right)^2 + \left(\frac{\partial P}{P}\right)^2} = \sqrt{\left(\frac{0.0067}{44100}\right)^2 + \left(\frac{0.0067}{840}\right)^2} = 8 \times 10^{-6}$$

4-uncertainty of air density ($\rho = \frac{p}{RT}$) : R=0.287 kJ/kg.K , p = 101.325 kpa= barometric pressure, T = Tambient = 293 K = 20°C.

$$\frac{\partial \rho}{\rho} = \sqrt{\left(\frac{\partial p}{p}\right)^2 + \left(\frac{\partial T}{T}\right)^2} = \sqrt{\left(\frac{1.5}{101.325}\right)^2 + \left(\frac{0.3}{20}\right)^2} = 0.021$$

5-Uncertainty of thermal conductivity of air k = 0.0257 × (T_f/293)^{0.86}.

$$\frac{\partial k}{k} = \sqrt{\left(\frac{\partial T_f}{T_f}\right)^2} = \sqrt{\left(\frac{0.1}{32.8}\right)^2} = 0.0033$$

6-Uncertainty of air velocity inside the air tunnel duct.

$$\frac{\partial v}{v} = \sqrt{\left(\frac{\partial v}{v}\right)^2} = \sqrt{\left(\frac{0.05}{6.0}\right)^2} = 0.0083$$

7-Uncertainty of the Reynolds number inside the duct.

$$\frac{\partial Re}{Re} = \sqrt{\left(\frac{\partial \rho}{\rho}\right)^2 + \left(\frac{\partial v}{v}\right)^2 + \left(\frac{\partial Dh}{Dh}\right)^2 + \left(\frac{\partial \mu}{\mu}\right)^2}$$

$$\frac{\partial Re}{Re} = \sqrt{(0.013)^2 + (0.008)^2 + \left(\frac{1}{230}\right)^2 + (0.0033)^2} = 0.066$$

8-Uncertainty of the dynamic viscosity of the air μ .

$$\frac{\partial \mu}{\mu} = \sqrt{\left(\frac{\partial T_f}{T_f}\right)^2} = \sqrt{\left(\frac{0.1}{32.8}\right)^2} = 0.0033$$

9-Uncertainty of the air mass flowrate.

$$\frac{\partial m}{m} = \sqrt{\left(\frac{\partial \rho}{\rho}\right)^2 + \left(\frac{\partial v}{v}\right)^2 + \left(\frac{\partial A}{A}\right)^2}$$

$$\frac{\partial m}{m} = \sqrt{\left(\frac{0.021}{1.23}\right)^2 + \left(\frac{0.05}{6}\right)^2 + \left(\frac{0.0067}{0.0441}\right)^2} = 0.15$$

10-Uncertainty of the heat exchanger effectiveness.

$$\frac{\partial \epsilon_s}{\epsilon_s} = \sqrt{\left(\frac{\partial T}{T}\right)^2} = \sqrt{\left(\frac{0.3}{50}\right)^2} = 0.006$$

where T represents the inlet and outlet air temperature to the heat exchanger.

11-Uncertainty of the evaporator and condenser heat energy.

$$\frac{\partial Q}{Q} = \sqrt{\left(\frac{\partial m}{m}\right)^2 + \left(\frac{\partial T}{T}\right)^2}$$

$$\frac{\partial Q}{Q} = \sqrt{\left(\frac{0.15}{0.1}\right)^2 + \left(\frac{0.3}{50}\right)^2} = 1.5$$

12-Uncertainty of the energy balance ratio (EBR).

$$\frac{\partial EBR}{EBR} = \sqrt{\left(\frac{\partial Q}{Q}\right)^2}$$

$$\frac{\partial EBR}{EBR} = \sqrt{\left(\frac{1.5}{400}\right)^2} = 0.00375$$

3. RESULTS AND DISCUSSION

3.1 Effect of Inlet Hot Air Temperatures on the Wickless Heat Pipe

Throughout the experimental tests of the wickless heat

pipe heat exchanger test rig, many parameters assist in representing the thermal performance of the present case Yinfeng et al. (2017). Figs. 4, 5 and 6 represent the temperature distributions of the used wickless heat pipe under full filling ratio (FR100%). The highest temperature values are generally located at the evaporator section of the wickless heat pipe for all examined cases. This is because this section is subjected to the hot air stream in the heat exchanger where additive amount of the hot air increases the heat accumulation on the outside wall of the evaporator section. Whereas the lowest values for the temperature are noted at the condenser section due to the cold air of the heat exchanger. Furthermore, the adiabatic section between the condenser and the evaporator sections has intermediate temperature values because this section hasn't heat addition or rejection.

The Figs. 4, 5 and 6 have a clear difference among the different inlet hot air; where highest values are achieved for the highest inlet hot air i.e. 60°C. This is because of the heat accumulation on the evaporator wall in the thermosiphon as compared to that accumulation for the case of the lower used hot air temperature. The additive amounts of the hot air acts on increasing the temperature of the wickless heat pipe wall. Regarding the mean values of the surface temperature of the studied wickless heat pipe, the highest mean value of the surface temperature may be noticed in Fig. 6 while the lower values are conducted for Figs. 5 and 4 respectively. This is because of increasing the air velocity in the heat exchanger where high air velocity (i.e. Fig. 6) form a high mass flow rate the order that makes the heat energy in which is subjected to the evaporator section is more. This thermal behaviour is notified incrementally in the Figs. 4 and 5, respectively. also, the previous thermal behaviour may be discussed according to the heat capacity concept, where more mass flow rate means more heat energy that will touch the surface area of the evaporator section of the studied heat pipe.

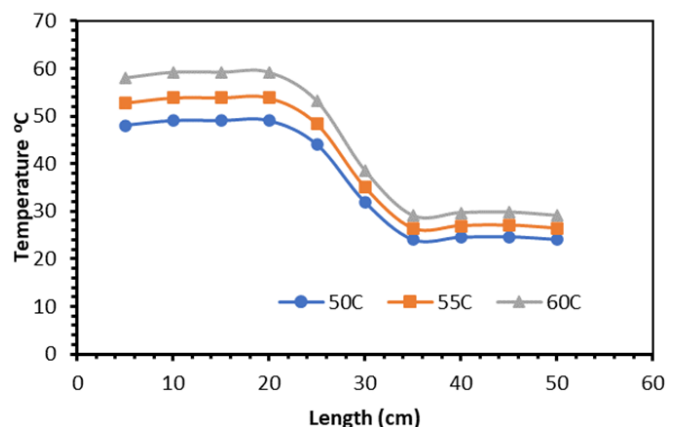


Fig. 4. Wickless heat pipe temperature distribution under different inlet air temperatures and velocity of 0.2 m/s and ethanol working fluid (FR100%)

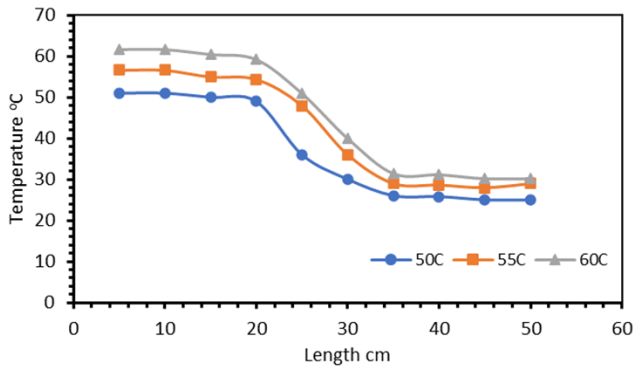


Fig. 5. Wickless heat pipe temperature distribution under different inlet air temperatures and velocity of 1 m/s and ethanol working fluid (FR 100%)

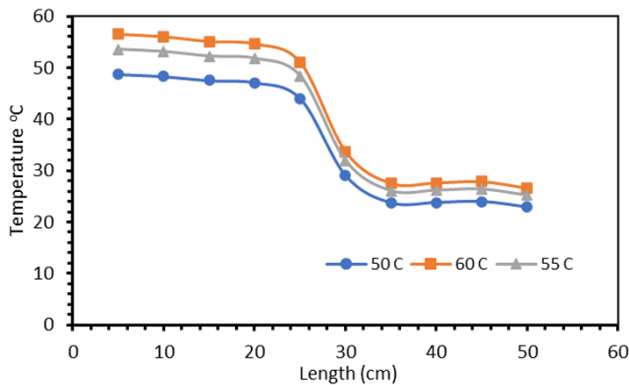


Fig. 6. Wickless heat pipe temperature distribution under different inlet air temperatures and velocity of 1.6 m/s and ethanol working fluid (FR 100%)

By regarding the working fluid types where Fig. 7 explains that the use of ethanol produces with lower surface temperature value along the wickless heat pipe length compared to the R1234-yf utilization. This is because of being the enthalpy of vaporization of R1234-yf is lower as compared to the ethanol working fluid as it is shown in table 4 below. The lower enthalpy heat of vaporization makes R1234-yf transfers lower value of heat energy the order that may tends to accumulate the heat energy over the external surface of the evaporator. Also, the higher enthalpy heat of vaporization makes a lot of vapor inside the wickless heat pipe where this one improves the heat transfer rate and reduces the heat accumulation effect. It is essential to set the operation conditions of both used working fluids inside the denoted heat pipe to investigate the pure effect of the used working fluids as shown in the Table 4 below. The variation among different inlet hot air temperatures subjected to the

evaporator section is extremely clear as shown in the Figs. 8 and 9.

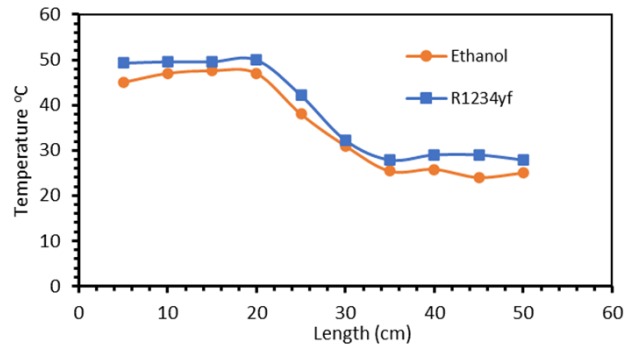


Fig. 7. Wickless heat pipe temperature distribution under different working fluid (FR 80%), velocity 1 m/s, inlet air temp = 50°C

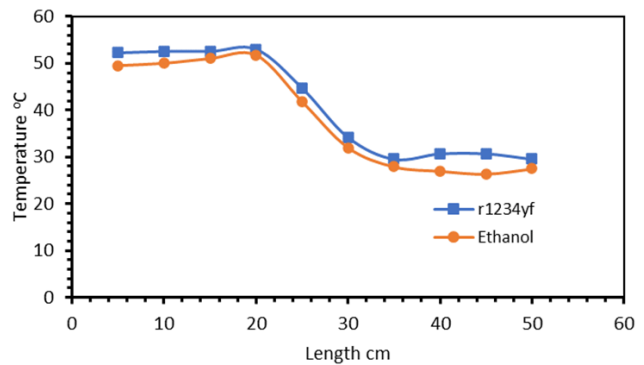


Fig. 8. Wickless heat pipe temperature distribution under different working fluid (FR 80%), velocity 1 m/s, inlet air temp = 55°C

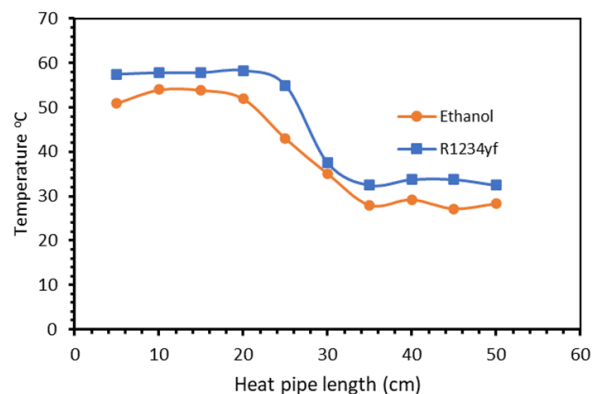


Fig. 9. Wickless heat pipe temperature distribution under different working fluid (FR 80%), velocity 1 m/s, inlet air temp = 60°C

Table 4. Working fluids thermodynamics-properties software

Working fluid	Thermosiphon-charged pressure kpa	Saturated temperature °C	Enthalpy of vaporization kJ/kg	Conductivity W/m.K
Ethanol	25	46.6	891.9	0.163
R1234-yf	1200	46.62	123.4	0.055

Fig. 10 represents the thermal performance of the wickless heat pipe under different filling ratios and ethanol utilization. It is noticed that the increase of the filling ratio makes an increase in the surface temperature of the heat pipe. This is considerable because of increasing the evaporated quantity of the working fluid inside the wickless heat pipe, increasing the active pressure inside the heat pipe and consequently enlarging the saturated temperature. The high saturated temperature means the vapour temperature is high therefore, the surface temperature of the used heat pipe is enlarged too. Thus, the higher filling ratio enhances the surface temperature as much as possible. This effect is clear for the case of R1234-yf utilization in the Fig. 11; the higher surface temperature is noted for high filling ratio compared to the lower one. The use of R1234-yf is considered modern in thermal research because it is modern refrigerant. So that, it is useful to provide a clear thermal performance for this type of refrigerant as compared to traditional working fluids like ethanol

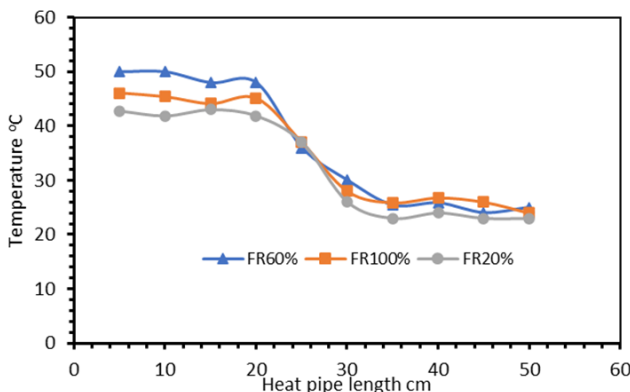


Fig. 10. wickless heat pipe temperature distribution under different filling ratio, Ethanol, velocity 1 m/s, inlet air temp = 50°C

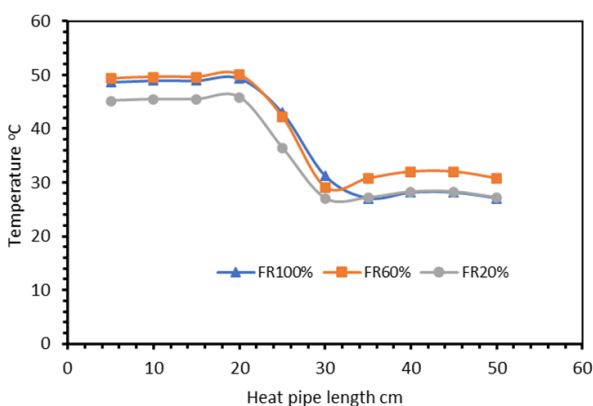


Fig. 11. Wickless heat pipe temperature distribution under different filling ratio, R1234-yf, velocity 1 m/s, inlet air temp = 50°C

3.2 Numerical Validation

The group of Figs. 12 that the experimental results of the wickless heat pipe temperature distribution have the same

trend for all cases of numerical computations. Furthermore, it is noted that the numerical results are higher than the experimental data because of the numerical computations do not reach the ideality of the experimental field. Moreover, the developed frictions between the air molecules and the wickless heat pipe acts on generating more heat energy. And as a results, there is no heat loss within the numerical analysis. Consequently, the higher values of numerical results are achieved as compared to the experimental results. The numerical results are extracted depending on Ansys Fluent R22.

3.3 Effectiveness

Heat exchanger is a device used in engineering applications to transfer heat energy from hot stream into cold stream. The present study introduces the heat exchanger function by depending on the thermal performance of the wickless heat pipe i.e. effectiveness Raghavendra et al. (2020). Figs. 13 (a) and (b) show the value of effectiveness for the studied wickless heat pipe heat exchanger under wide range of Reynolds number and filling ratio values. The general trend achieves an enhancement in the effectiveness up to Reynolds number value of 10332 where this enhanced trend is conducted for all studied filling ratio values. Moreover, an obvious reduction in the effectiveness of the wickless heat pipe heat exchanger is observed after the peak point i.e. after Reynolds number value of 10332; where this trend is carrying on up to the last tested Reynolds number. The first half of the Figs. 13 (a) and (b) i.e. (the enhancement trend) is executed due to increasing the mass flow rate of the hot and cold air in the ducts; where higher mass flow rate acts on eliminating the thermal bounded layers over the surfaces of the wickless heat pipe sections. Therefore, more heat transfer rates are conducted from the condenser section wall to the cold air and from the hot air to the evaporator section of the studied heat pipe. It is well known that the improved heat transfer rate between the wickless heat pipe sections and the air paths of the heat exchanger achieves an obvious temperature difference between the inlet and outlet air of the studied heat exchanger the order that improves the effectiveness values.

Meanwhile, the second half of Figs. 13 (a) and (b) that refer to the reduction in the effectiveness values with respect to Reynolds number may be executed due to increasing the separation area between the air flow and surface of the evaporator and condenser sections respectively. The separation may be conformed due to increasing the Reynolds number due to increasing the air flow velocity. Moreover, the higher Reynolds number may conduct high friction losses between the air and the surfaces of the wickless heat pipe. Higher Reynolds number makes higher frictions and, consequently, higher thermal bounded layers, which resists the heat transfer between heat pipe surface and the air streams.

Also, it is conducted that the best effectiveness of the heat pipe heat exchanger is presented at the filling ratio of 60%.

This is the outcome is because the available working fluid mass for filling ratio of 60% reaches the best phase change process i.e. the equivalent amount of evaporated liquid that corresponds to one of condensed vapour. Moreover, the amount of the generated vapor at best filling ratio could transfer the heat energy to the condenser side more appropriately as compared to other filling ratio values.

By considering the R1234-yf utilization; Fig. 13 (b) refers to the heat pipe heat exchanger effectiveness under the same

filling ratios and Reynolds number range. The general trend is the same as the ethanol usage trend because of being the boundary conditions and the rig geometries remain as the same also, the best operation cases are denoted at the filling ratio of 60% under Reynolds number of 10332. The obvious difference in Fig. 13 (b) is the peak value of the effectiveness where the use of R1234-yf working fluid generates low effectiveness values due to the enthalpy of vaporization effect, i.e. Table 4.

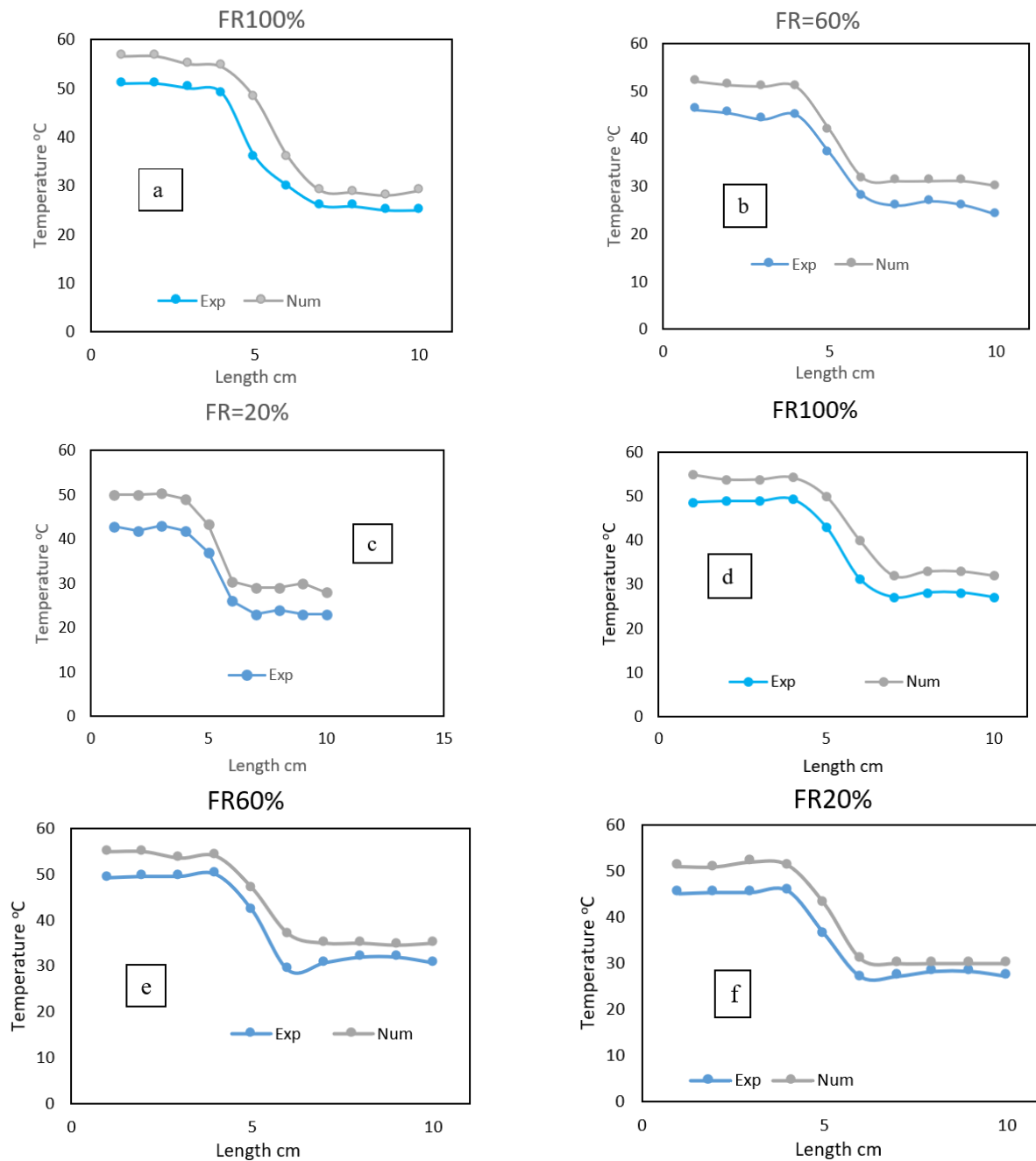


Fig. 12. (a-c) The validation between experimental results and numerical results at $Re = 10233$, inlet hot air temp. = $50\text{ }^{\circ}\text{C}$, Ethanol; (d-f) The validation between experimental results and numerical results at $Re = 10233$, inlet hot air temp. = $50\text{ }^{\circ}\text{C}$, R1234-yf

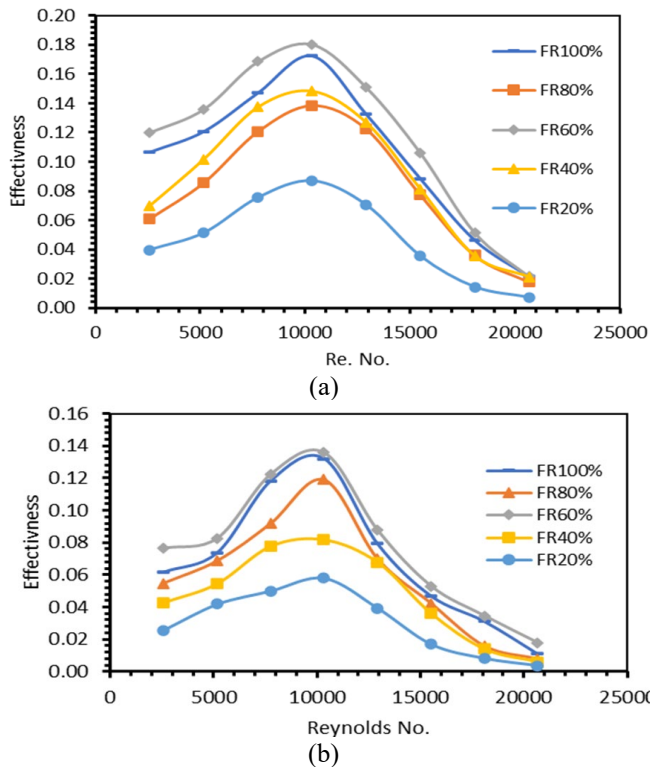


Fig. 13. (a) Wickless heat pipe heat exchanger effectiveness under different Reynolds number and filling ratios and the use of ethanol as working fluid; (b) Wickless heat pipe heat exchanger effectiveness under different Reynolds number and filling ratios and the use of R1234-yf as the working fluid

It is essential to implement the effect of the inlet hot air temperature on the effectiveness value where the Fig. 14 shows that the higher input air temperature achieves higher values of the heat exchanger effectiveness obviously. This is because of the effectiveness depends on the input and output temperatures of the air streams. Therefore, and considering that the cold air temperature remains the same during all the tests. So that, the effectiveness values achieve a direct proportion to the hot air input temperature.

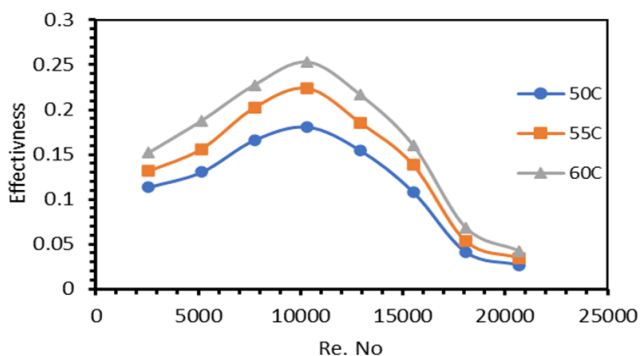


Fig. 14. Wickless heat pipe heat exchanger under different input temperature of the hot duct and filling ratio of 60% of the ethanol working fluid

Furthermore, it is found that the same as trend of the effectiveness values are conducted when the R1234-yf working fluid to be utilized, as shown in the Fig. 15. The minimum values are denoted when the input hot air temperature is 50°C. while the maximum range is reached for the highest input air temperature i.e. 60°C. The main difference between the two working fluids used is the peak value of the effectiveness where it is conducted for the ethanol compared to the R1234-yf. The prime reason for this status may be due to the effect of the enthalpy on vaporization and thermal conductivity. So, the highest values of the denoted thermo-physical properties are more satisfied for ethanol working fluid than for R1234-yf.

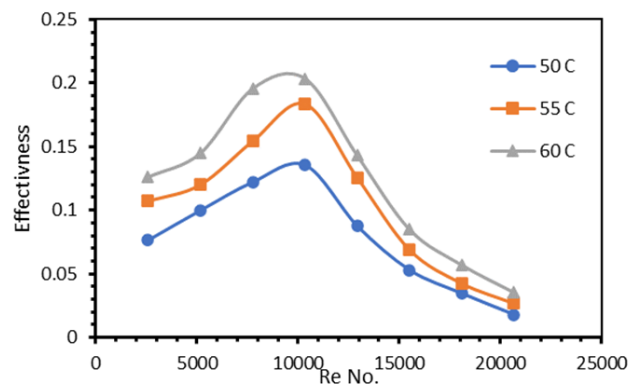


Fig. 15. Wickless heat pipe heat exchanger under different input temperature of the hot duct and filling ratio of 60% of the R1234-yf working fluid

3.3 Energy Balance Ratio (EBR)

Figs. 16 and 17 represent the wickless heat pipe performance's EBRs (Abdallah et al., 2022). This EBR is a ratio between the consumed heat energy at the evaporator section to the rejected one at the condenser section of the heat exchanger duct. The unity is the optimum value for the studied cases because it refers to the idealist of the heat pipe operation. The EBR performance in the case of using the ethanol working fluid is satisfied the performance of the effectiveness under the same operation condition also the obtained results explain that the best EBR is attained at the Re number of 10332. While, the lower values of the Re number operation conditions are satisfied a less EBR values. The increase of the EBR values up to the Re of 10332 is due to enhancing the heat transfer rate inside the wickless heat pipe, satisfying the increasing mass flow rate of the hot and cold air in the heat exchanger. Whereas the reduction in the EBR value after Re of 10332 may be due to the separation between the air of the heat exchanger ducts and the surface area of the studied wickless heat pipe. Also, more mass flow rate tends to increase the friction over the surfaces of the condenser and evaporator of the wickless heat pipe. The last one fabricates an increase in the thermal bounded layer at that denoted surface area the order that eliminates the heat transfer rate between the air and the heat pipe active sections i.e. evaporator and condenser sections. It is essential to

know that the best EBR values have been executed at filling ratio of 60% where this achievement may be due to idealizing the evaporation and condensation of the used working fluid inside the heat pipe.

Regarding the R1234-yf utilization effect, the EBR results showed the same trend of the ethanol under the same operating conditions of filling ratios and Reynolds number. It is clear that the developed results in Fig. 17 satisfied the same range of the best EBR when the filling ratio is reached the 60% while the lowest values are indicated for the lower filling ratios of 40% and 20%, respectively. The worst thermal performance of the EBR is more clear in the case of using R1234-yf as compared to ethanol usage. This is because of the reduction in the enthalpy of vaporization that limits the heat transfer rate throughout the wickless heat pipe and so on the overall heat exchanger. Furthermore, the perfect values of the EBR for both types of the used working fluids are approached to be closed due to the similarity of the surface area of the wickless heat pipe and the operation conditions.

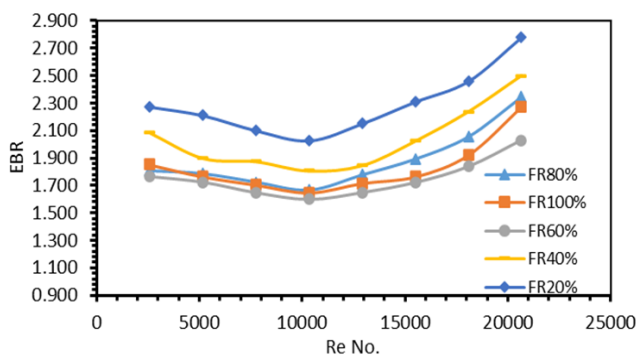


Fig. 16. Wickless heat pipe heat exchanger EBR under different Reynolds number and filling ratios and the use of Ethanol as working fluid

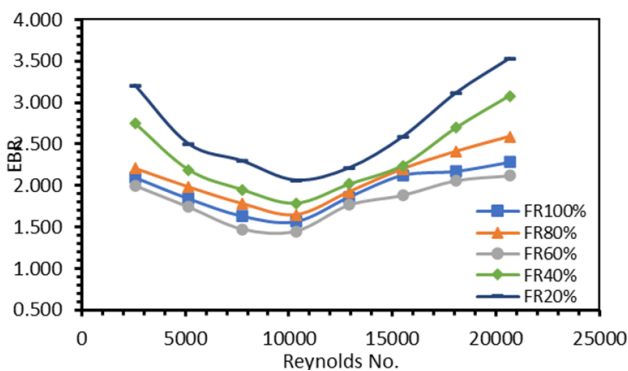


Fig. 17. Wickless heat pipe heat exchanger EBR under different Reynolds number and filling ratios and the use of R1234-yf as working fluid

3.4 Z-factor

By referring to the overall thermal performance of the studied wickless heat pipe heat exchanger, it is essential to develop an optimization to get on the best performance

conditions in which it can be used to enhance, operate and develop this type of application in the next studies. Consequently, a Z-factor is proposed for this aim, where this factor is a dimensionless term that expresses the ratio between the effectiveness and the EBR of the studied test rig. The z-factor is a ratio between effectiveness and EBR; where the ideal case is attained when the heat energy consumed in the hot duct equals rejected heat energy in the cold duct, the order that makes EBR reaches unity and effectiveness achieves 100%. Fig. 18 shows that the optimum operation conditions that attains the Z-factor's maximum values are denoted at a Reynolds number of 10332. Fig. 18 presents an enhancement in the relation between the Z-factor and the Reynolds number up to reaching the best value of the Z-factor at the Reynolds number of 10233. Also, an obvious reduction in the Z-factor values has been attained with increasing the Reynolds number to more than 10322. The higher Reynolds number which reduced the Z-factor, is a result of adding more frictions between the air and the surfaces of the wickless heat the order that may enlarge the thermal bounded layers. Moreover, the higher Reynolds number mean additive separation between the air and the contact surface area of the denoted heat pipe. The use of ethanol working fluid presents the best values of the Z-factor as compared to the R1234-yf utilization, where this trend is satisfying the obtained thermal behavior of effectiveness and EBR, respectively because of the enthalpy heat of vaporization and thermal conductivity of the referred used working fluids.

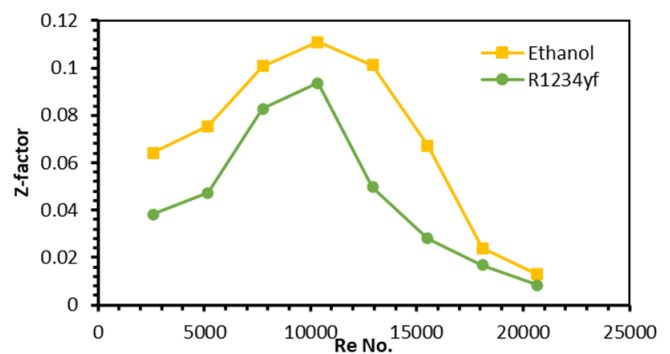


Fig. 18. The performance of Z-factor to the Reynolds number and two different types of working fluids

3.5 Contributed Studies

It is essential to improve the present work by make a comparison present work's reliability by comparing it with related previous studies with nearest boundary conditions or geometries. So that, Fig. 19 attaches the temperature distribution of the long-length wickless heat pipe under different usage of the working fluid. The related studies of Naresh and Balaji (2017) and Abdallah et al. (2022) presented lower temperature values along the heat pipe because of using the water as working fluid throughout the refereed study. The water thermo-physical properties are more efficient, such as enthalpy heat of vaporization and

thermal conductivity, which tend to augment the heat transfer inside the wickless heat pipe. Therefore, the temperature of ethanol or R1234-yf usage status is higher because these fluids have lower thermophysical properties concerning water.

Regarding the whole system i.e. wickless heat pipe heat exchanger where the Fig. 20 indicates that the effectiveness tends to be increased by increasing the temperature of the inlet hot air. This enhancement is observed for the present study cases that include ethanol and R1234-yf for the elated study of Ayad et al. (2022). It is also, conducted that the effectiveness value of the compared with study is more than that of the present study. This divergence is a results of being that there is 4 rows of wickless heat pipe in the related study while, the present study includes just one wickless heat pipe. This difference obviously changes the effectiveness value as shown in the Fig. 20.

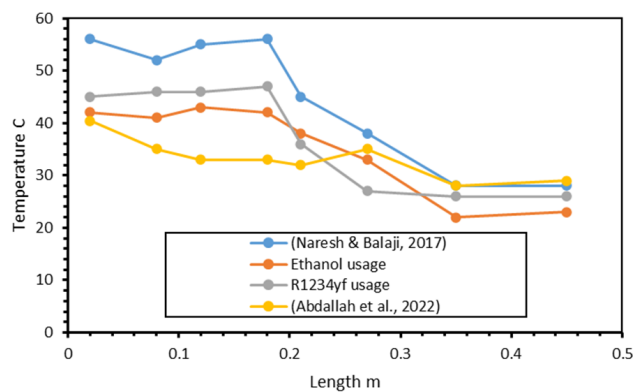


Fig. 19. Temperature distribution along wickless heat pipe at FR = 20% and for different studies

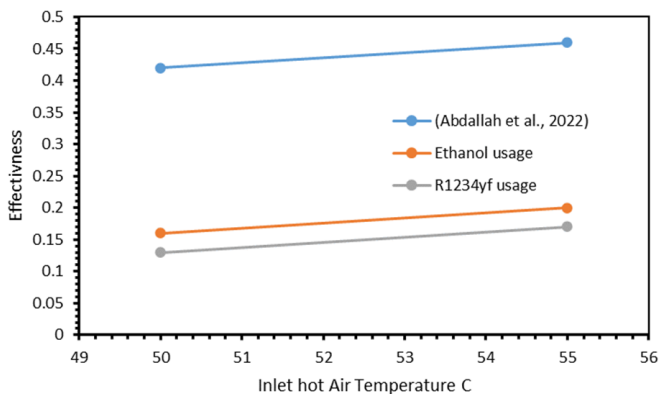


Fig. 20. Effectiveness comparison for related studies at air velocity of 1 m/s

4. CONCLUSION

The present study achieved the thermal performance of the wickless heat pipe heat exchanger under different operations conditions in the hot and cold air paths. Also, different working fluid types and filling ratio values have been charged inside the used wickless heat pipe. Thus, the

outcomes refers that The selection of the working fluid type that is used in the wickless heat pipe is the prime mover of changing the thermal performance of the wickless heat pipe – heat exchanger application. Therefore, the use of ethanol working fluid performed best compared to the R1234-yf usage, which is obvious by depending on Z-factor. Also, charging the denoted heat pipe with a filling ratio of 60% improves the wickless heat pipe heat exchanger effectiveness to reach 0.182 and 0.135 using ethanol and R1234-yf, respectively.

REFERENCES

- Abdallah, A.S., Yasin, N.J., Ameen, H.A. 2022. Thermal performance enhancement of heat pipe heat exchanger in the air-conditioning system by using nanofluid. *Frontiers in Heat and Mass Transfer*, 18.
- Abreu, S.L., Colle, S. 2004. An experimental study of two-phase closed thermosyphons for compact solar domestic hot-water systems. *Solar Energy*, 76, 141–145.
- Alizadehdakheel, A., Rahimi, M., Alsairafi, A.A. 2010. CFD modeling of flow and heat transfer in a thermosyphon. *International Communications in Heat and Mass Transfer*, 37, 312–318.
- Bhatia, A. 2001. HVAC-How to size and design ducts. *Continuing Education and Development, Inc.*, 877, 89.
- Çengel, Y.A. 2009. Heat exchangers. In *Heat Transfer Engineering*, 609–662.
- Chen, R.H., Su, G.H., Qiu, S.Z., Fukuda, K. 2010. Prediction of CHF in concentric-tube open thermosiphon using artificial neural network and genetic algorithm. *Heat and Mass Transfer*, 46, 345–353.
- Eidan, A.A., Najim, S.E., Jalil, J.M. 2016. Experimental and numerical investigation of thermosyphone performance in HVAC system applications. *Heat and Mass Transfer*, 52, 2879–2893.
- Guo, W., Nutter, D.W. 2009. An experimental study of axial conduction through a thermosyphon pipe wall. *Applied Thermal Engineering*, 29, 3536–3541.
- Haider, S.I., Joshi, Y.K., Nakayama, W. 2002. A natural circulation model of the closed loop, two-phase thermosyphon for electronics cooling. *Journal of Heat Transfer*, 124, 881–890.
- Hussein, H.M.S., El-Ghetany, H.H., Nada, S.A. 2006. Performance of wickless heat pipe flat plate solar collectors having different pipes cross sections geometries and filling ratios. *Energy Conversion and Management*, 47, 1539–1549.
- Jafari, D., Filippeschi, S., Franco, A., Di Marco, P. 2017. Unsteady experimental and numerical analysis of a two-phase closed thermosyphon at different filling ratios. *Experimental Thermal and Fluid Science*, 81, 164–174.
- Jia, R., Wang, Y., Shi, H., Xiong, J. 2014. Experimental and numerical study on the self-balancing heating performance of a thermosyphon during the process of oil production. *Applied Thermal Engineering*, 73, 1270–

- 1278.
- Jouhara, H., Robinson, A.J. 2009. An experimental study of small-diameter wickless heat pipes operating in the temperature range 200°C to 450°C. *Heat Transfer Engineering*, 30, 1041–1048.
- Kim, Y., Kim, J.S., Shin, D.H., You, S.M., Lee, J. 2020. Enhanced thermal performance of a thermosyphon for waste heat recovery: Microporous coating at evaporator and hydrophobic coating at condenser. *Applied Thermal Engineering*, 175, 115332.
- Klein, S.A., Alvarado, F. 2013. Engineering equation solver software (EES). F-Chart Software: Madison, WI, USA.
- Kundu, B., Das, P.K. 2009. Performance and optimum design analysis of convective fin arrays attached to flat and curved primary surfaces. *International Journal of Refrigeration*, 32, 430–443.
- Liu, Y., Li, Z., Li, Y., Jiang, Y., Tang, D. 2019. Heat transfer and instability characteristics of a loop thermosyphon with wide range of filling ratios. *Applied Thermal Engineering*, 151, 262–271.
- Narcy, M., Lips, S., Sartre, V. 2018. Experimental investigation of a confined flat two-phase thermosyphon for electronics cooling. *Experimental Thermal and Fluid Science*, 96, 516–529.
- Naresh, Y., Balaji, C. 2017. Experimental investigations of heat transfer from an internally finned two phase closed thermosyphon. *Applied Thermal Engineering*, 112, 1658–1666.
- Noie, S.H. 2005. Heat transfer characteristics of a two-phase closed thermosyphon. *Applied Thermal Engineering*, 25, 495–506.
- Ochsner, K. 2008. Carbon dioxide heat pipe in conjunction with a ground source heat pump (GSHP). *Applied Thermal Engineering*, 28, 2077–2082.
- Ozsoy, A., Yildirim, R. 2016. Prevention of icing with ground source heat pipe: A theoretical analysis for Turkey's climatic conditions. *Cold Regions Science and Technology*, 125, 65–71.
- Raad, O. 2019. The improvement of the solar air heater duct by wired ribs utilization. *Karbala International Journal of Modern Science*, 5, Article 6.
- Raghavendra, C.R., Hasavimath, K., Naik, K. 2021. Study on effectiveness of heat pipe heat exchanger with copper tube cylinders. *Materials Today: Proceedings*, 39, 800–804.
- Sabharwall, P., Gunnerson, F. 2009. Engineering design elements of a two-phase thermosyphon for the purpose of transferring NGNP thermal energy to a hydrogen plant. *Nuclear Engineering and Design*, 239, 2293–2301.
- Samba, A., Louahli-Gualous, H., Le Masson, S., Nörterhäuser, D. 2013. Two-phase thermosyphon loop for cooling outdoor telecommunication equipments. *Applied Thermal Engineering*, 50, 1351–1360.
- Sarafraz, M.M., Tlili, I., Tian, Z., Bakouri, M., Safaei, M.R. 2019. Smart optimization of a thermosyphon heat pipe for an evacuated tube solar collector using response surface methodology (RSM). *Physica A: Statistical Mechanics and Its Applications*, 534, 122146.
- Seo, J., Bang, I.C., Lee, J.Y. 2016. Length effect on entrainment limit of large-L/D vertical heat pipe. *International Journal of Heat and Mass Transfer*, 97, 751–759.
- Sulaiman, M.W., Daraghme, H.M., Wang, C.C. 2020. Energy-saving potential of separated two-phase thermosiphon loops for data center cooling. *Journal of Thermal Analysis and Calorimetry*, 141, 245–265.
- Tong, Z., Liu, X. H., Li, Z., Jiang, Y. 2016. Experimental study on the effect of fill ratio on an R744 two-phase thermosyphon loop. *Applied Thermal Engineering*, 99, 302–312.
- Xu, Z., Zhang, Y., Li, B., Wang, C.C., Li, Y. 2018. The influences of the inclination angle and evaporator wettability on the heat performance of a thermosyphon by simulation and experiment. *International Journal of Heat and Mass Transfer*, 116, 675–684.
- Yang, X., Guo, J., Yang, B., Cheng, H., Wei, P., He, Y.L. 2020. Design of non-uniformly distributed annular fins for a shell-and-tube thermal energy storage unit. *Applied Energy*, 279, 115772.
- Wang, Y., Wang, X., Chen, H., Taylor, R.A., Zhu, Y. 2017. A combined CFD/visualized investigation of two-phase heat and mass transfer inside a horizontal loop thermosiphon. *International Journal of Heat and Mass Transfer*, 112, 607–619.